DOE/ER10367-1

UPPER-BOUND SOLUTIONS TO FLOW THROUGH CONICAL CONVERGING DIES

by

B. Avitzur, C. Narayan, and Y.T. Chou

Department of Metallurgy and Materials Engineering

Lehigh University

September, 1980

DISCLAIMER

TABLE OF CONTENTS

NOMENCLATURE

b	see Figs. 4 and 5
e	distance from apex to the axis of symmetry (Fig. 2d)
f, g, F	function
I_1, I_2	definite integrals (Eqs. 14a and b)
J^*	upper bound on power
K	a constant (see Eq. 16)
ℓ_1, ℓ_2	see Fig. 5
L	length of land of the die
m	friction factor
O	apex of the cone of die
P	point on the axis of symmetry (Fig. 2c)
r, θ, ϕ	axes of spherical coordinate system
r_o^*	radial distance of a point entering the deformation region
r_f^*	radial distance of a point exiting the deformation region
R, θ, x	axes of cylindrical coordinate system
R_d	see Fig. 6
R_γ	radius of the die at $x = 0$
R_o	initial radius of rod
R_f	final radius of rod
R_1	radius of cylindrical raw material
R_2	radius of cylindrical product
$\dot{U}_r, \dot{U}_\theta, \dot{U}_\phi$	components of velocity vector in spherical coordinate system

v_o	velocity of incoming flow
v_f	velocity of exiting flow
Δv	velocity discontinuity
V	volume of deformation zone
$\dot{V}$	volume rate
$\dot{W}_f$	power to overcome friction losses
$\dot{W}_i$	power of internal deformation
$\dot{W}_s$	power to overcome shear
α	semicone angle of the die
β	angle between the surface of velocity discontinuity and the axis of symmetry
Γ_i	surface of velocity discontinuity
$\dot{\varepsilon}_{ij}$	strain rate
$\dot{\varepsilon}_{rr}$, $\dot{\varepsilon}_{\theta\theta}$, $\dot{\varepsilon}_{\phi\phi}$	components of strain rate in spherical coordinate system
$\dot{\varepsilon}_{RR}$, $\dot{\varepsilon}_{\theta\theta}$, $\dot{\varepsilon}_{xx}$	components of strain rate in cylindrical coordinate system
σ_o	yield limit in uniaxial tensile test
σ_{xb}	extrusion stress (back pull stress)
σ_{xf}	drawing stress (front pull stress)
ψ	function
0, Δ, $\square$	symbols indicating spherical, triangular, and trapezoidal velocity fields, respectively

ABSTRACT

Limit analysis is a very versatile modeling technique that can be used to study metal-forming processes. The upper-bound analysis can be used to predict an upper limit on the power requirements. This work reviews some upper-bound solutions that describe flow through conical converging dies. The concept of a trapezoidal field is introduced and dealt with in great detail, and the power requirements based on the trapezoidal field are calculated. The results are compared with those obtained using spherical and triangular fields. The relative stress expression has been developed analytically and the final optimization with respect to the pseudoindependent parameter is done numerically. The trapezoidal field predicts a lower upper-bound solution for small semicone angles. The range over which the trapezoidal field solution becomes dominant increases with increasing friction factor.

LIST OF FIGURES

INTRODUCTION

Foreword

The operations called wire drawing, rod extrusion, hydrostatic extrusion, and tube sinking are all performed through similar dies. Identical flow patterns are assumed in the analytical study of these different processes. Therefore, the analysis described here and the flow characteristics which are discussed can be utilized in dealing with several different processes. A wire, or a rod, of initial radius R_o is pushed (extruded) or pulled (drawn) through a conical portion of a die (see Fig. 1). As it passes through the die, the wire deforms plastically and decreases in diameter. Although the cylindrical portion of the die causes additional friction losses, it is, nevertheless, required for dimensional stability of the product of the final radius R_f, and also because of die manufacturing practice. An upper-bound solution for the case of constant shear friction factor is derived simultaneously for the power involved in drawing and in extrusion. At the vicinity of the die, the wire undergoes plastic deformation. Further away, at the entrance and exit of the die, the incoming workpiece and the product, respectively, move as two rigid bodies in a direction parallel to the axis of symmetry. The incoming rod moves at the velocity v_o and the product at the velocity v_f. This is a steady state process; therefore, when a sound product is produced, the law of incompressibility dictates that

$$\frac{v_f}{v_o} = \left(\frac{R_o}{R_f}\right)^2 \tag{1}$$

When sound flow is maintained and a sound product is manufactured, it can be noted that any concentric cylinder of the radius R_1 in the raw material will end up as a concentric cylinder in the product. Volume constancy dictates that the ratio of the radius of the cylinder on the product (R_2) to that of the cylinder at the entrance (R_1) will equal the ratio of the radius of the product to that of the entering rod,

$$\frac{R_2}{R_1} = \frac{R_f}{R_o} \tag{2}$$

In the present study, a number of flow patterns within the deformation regions are explored. The relationships of the boundaries between the deformation region and its rigid body neighbors at the entrance and exit of the die to the characteristics of several flow patterns are investigated. The effectiveness of the several modes of deformation as models resembling the actual process is studied.

In the application of upper-bound solutions to the metal-forming processes that employ flow through conical converging dies, several velocity fields can be explored. Some of the literature that provide established solutions will be presented, and new solutions will be developed. In this introduction, classification of a wide range of kinematically admissible velocity fields is proposed. The first section, described in Fig. 2, presents basic simple fields.

Next, some assembly arrangements of the simple fields that cover the entire deformation region by a combination of several of the above-mentioned simple fields are described. As the assembly becomes more complex, the treatment gets closer and closer to the treatment of metal-forming by

numerical methods; specifically, the finite element method and the "Upper-Bound Elemental Technique," (UBET).

In the above-mentioned assembly of units, the individual simple units cover the entire deformation region without overlapping. At the end of this section, the concept of overlapping regions is introduced. The power of this concept in introducing variability to the family of velocity fields is demonstrated.

Classification of Basic Fields

General Observations

In the present study, the boundaries between the deformation region (zone II where plastic flow occurs) and its rigid neighbors at the entrance and exit of the die (zones I and III respectively), are surfaces of velocity discontinuity, Γ_2 and Γ_1 respectively (see Fig. 1b). A general flow pattern is described by the flow line in Fig. 1b. Here, point A, at a radial distance R_1, from the axis of symmetry, moves towards the die at a velocity v_o until it reaches the surface of velocity discontinuity Γ_2. Undergoing a drastic change in direction and magnitude, the point crosses the surface Γ_2, enters the deformation region (zone II) and moves in a generally converging flow towards the exit at an accelerated speed. The path of flow through the deformation region (zone II) is described here as a winding general hypothetical path. On reaching the surface of velocity discontinuity Γ_1 at the exit, another change in direction and magnitude of the velocity vector occurs, and the point, on crossing Γ_1, proceeds to move parallel to the axis of symmetry at the constant rigid body speed of v_f.

The radial distance of the point when it enters zone III is R_2, dictated by Eq. (2) to be $R_2/R_1 = R_f/R_o$.

The points along the path of flow where drastic changes in the velocity vector occur, that is, where point A crosses the surfaces of velocity discontinuity Γ_2 and Γ_1, are noted in Fig. 1b. These two points are connected by a straight line which is extended to its intersection with the axis of symmetry of the workpiece and die. The intersection point is denoted by O, and the radial distance of the two points on Γ_2 and Γ_1 respectively from O are denoted as the distances r_o^* and r_f^*. From geometrical similarity and by Eq. (2) it is observed that

$$\frac{r_o^*}{r_f^*} = \frac{R_1}{R_2} = \frac{R_o}{R_f} \tag{3}$$

The two surfaces, Γ_1 and Γ_2, are "conjugating surfaces," related to each other by Eq. (3). This observation is most useful in further derivations, especially during the volume integration performed to determine the internal power of deformation in the deformation region.

The basic units of flow modes that are described in this manuscript maintain only straight-line flow in the deformation region. Thus, for solid rod, but not for tube, the conjugation rule provided by Eq. (3) takes on a simple significance and is described with each individual field.

Surfaces of Velocity Discontinuity

The velocity field described in Fig. 1b is a radially converging flow directed into the apex of the die (O). The two surfaces of velocity discontinuity, Γ_1 and Γ_2, are 'parallel' so that the ratio of the radial

distance (r_o^*) of a point entering the deformation region to its radial distance (r_f^*) exiting the deformation region is equal to the ratio R_o/R_f. The angular position θ remains constant for each point while it is passing through the plastic region. The angle β that the tangential line to the curved surface of discontinuity makes with the axes of symmetry may be chosen as an arbitrary function of the angular position θ. The velocity of the point entering the deformation region with coordinates r_o^* and θ is

$$\dot{U}_r\Big|_{\Gamma_2} = v_o \frac{\sin \beta}{\sin (\beta+\theta)} \tag{4}$$

In the deformation region, radially converging flow coupled with the law of incompressibility leads to

$$\dot{U}_r = \dot{U}_r\Big|_{\Gamma_2} \left(\frac{r_o^*}{r}\right)^2 = v_o r_o^{*2} \frac{\sin \beta}{r^2 \sin(\beta+\theta)}$$

$$= v_f \left(\frac{r_f^*}{r}\right)^2 \frac{\sin \beta}{\sin(\beta+\theta)} \tag{5a}$$

Note that for the spherical field, Eq. (5a) reduces to

$$\dot{U}_r = v_f \left(\frac{r_f}{r}\right)^2 \cos \theta \tag{5b}$$

Along surface Γ_1 and Γ_2, the velocity discontinuities are

$$\Delta v\Big|_{\Gamma_2} = v_o \cos \beta - \dot{U}_r \cos (\beta+\theta) = v_o[\cos \beta + \sin \beta \cot (\beta+\theta)]$$

$$\Delta v\Big|_{\Gamma_1} = v_f[\cos \beta + \sin \beta \cot (\beta+\theta)] \tag{6a}$$

For the spherical velocity field

$$\Delta v|_{\Gamma_1} = v_o \cos \beta \equiv v_o \sin \theta$$
$$\Delta v|_{\Gamma_1} = v_f \sin \theta \qquad (6b)$$

Because r_f^* in Eq. (5a) is yet an arbitrary function of θ, ($r_f^* = r_f^*(\theta)$), the determination of the strain rate components by applying Eq. (8.1) of Ref. 3 to Eq.(5a) is not performed here. When any specific functional relation of r_f^* to θ is determined, the strain rate components are derivable.

The basic modes of converging flow described in Fig. 2 can be classified in three categories, i.e. as:

1. Conically converging radial flow
2. Cylindrically converging radial flow, and
3. Parallel Flow.

1. Conically Converging Radial Flow

In the general conically converging radial flow (Fig. 2a), any point in the deformation zone II moves towards the apex of the die, **O**, along a straight line which forms the angle θ with the axis of symmetry of the workpiece and die. A generally winding shape of one surface of velocity discontinuity, say surface Γ_1, is admissible, dictating the shape of the other conjugate surface through Eq. (3). These surfaces are called "conjugating similar surfaces." The shapes of the surfaces of velocity discontinuity dictate the dependence of r_o^* and r_f^* on the angle θ.

In the basic unit fields covered in this paper, two specific shapes of the surfaces of velocity discontinuity are considered. First the spherical

surfaces of velocity fields associated with the so-called "spherical velocity field" denoted from here on by (0) (see Refs. 1, 2 and 3) are presented. Here, the surfaces Γ_1 and Γ_2 are two concentric spherical surfaces with their center at the apex (0) of the die. The radial distances r_o^* and r_f^* become constants r_o and r_f respectively, rendering the radial distances r_o and r_f independent of θ. The spherical velocity field is a rigid single field, not a family of fields, and has no pseudoindependent parameter by which the computed power can be minimized.

The second specific field in the category of conically converging radial flows is the "trapezoidal" field (⏢) with parallel surfaces Γ_1 and Γ_2 inclined to the axis of symmetry at an arbitrary angle β. The treatment of this field is developed in this manuscript. The angle β becomes a pseudoindependent parameter subject to optimization. The treatment of the trapezoidal field for drawing and extrusion in plane strain is presented in Refs. 4 and 5.

2. Cylindrically Converging Radial Flow

The cylindrically converging basic units (Fig. 2b) as described in Chapter 7 of Ref. 3 are rectangular and right-angle triangular rings, and solid cylindrical discs. These units, as individuals, do not serve as a field that leads to an upper-bound solution for flow through conical converging dies. In combination with each other or with other units however, this assembly of units can lead to an upper-bound solution by a method called UBET (see Ref. 6). For the sake of brevity, the above-mentioned rings and discs will not be covered in this paper.

3. Parallel Flow

In the parallel flow, any point in the deformation region (Fig. 2c) is moving along a straight line parallel to the surface Γ_3, which may be the surface of the die. In a more complex assembly of units, the surface Γ_3 may be an interface between two fields.

The surfaces Γ_1 and Γ_2 can be curved as long as the vertices (edges) are at the entrance, the exit and on the axis of symmetry, point P, respectively, and the ratio of $r_o^*/r_f^* = R_o/R_f$ (Eq. (3)) is obtained for each point passing through the deformation region. These surfaces (Γ_1 and Γ_2) are called "conjugate intersecting surfaces." The radial distances r_o^* and r_f^* become a general function of the position of the moving apex 0. In this paper, the surfaces Γ_1 and Γ_2 are handled only as straight lines and the position of the vertex P is treated as a pseudoindependent parameter, subject to optimization. The field is called the "triangular" field denoted by (Δ).

4. The Toroidal Flow

In the toroidal flow (Fig. 2d), the straight line flow is directed towards the apex 0, which is a circle of a radius e lying on the extension of the conical surface Γ_3. One surface (Γ_2 or Γ_1) may be a toroidal surface with the center at 0, but then the other surface (Γ_1 or Γ_2 respectively) becomes a complex function of e and θ. Work now in progress on this field shows that it applies to the analysis of tubes, but leads to singularity problems when θ approaches zero for finite non-zero values of e. The complexity of the solution excludes the treatment of the toroidal field from this paper.

Individual Basic Fields

The following is a more detailed description of the individual basic velocity fields.

1. Conically Converging Velocity Fields

1.1 The Spherical Velocity Field

One of the earlier proposed fields, the spherical field is described in Refs. 1, 2 and 3 as follows:

A kinematically admissible velocity field is described in Fig. 3. The wire is divided into three regions in which the velocity field is continuous. In zones I and III the velocity is uniform and has only an axial component. In zone I the velocity is v_o, and in zone III the velocity is v_f. Because of volume constancy, Eq. (1) dictates that

$$v_o = v_f \left(\frac{R_f}{R_o}\right)^2$$

In zone I, deformation has not yet begun. It consists of the incoming rod, which is separated from the deforming zone II by the surface Γ_2. Surface Γ_2 is spherical, of radius r_o with the origin at the apex 0 of the cone of the die. Zone II is the zone of deformation bounded by the surface of the die, with a cone of an included angle 2α and two concentric spherical surfaces Γ_1 and Γ_2. The surface Γ_2 is the previously mentioned spherical boundary between zones I and II. The spherical surface Γ_1 of radius r_f, with the origin at the apex 0 of the cone, separates zone II from the emerging product of zone III. In zone II the velocity is directed toward the apex 0 of the cone, with cylindrical symmetry.

In the spherical coordinate system (r,θ,ϕ), the velocity components are

$$\dot{U}_r = v = - v_f r_f^2 \frac{\cos \theta}{r^2} \qquad \dot{U}_\theta = \dot{U}_\phi = 0 \tag{7}$$

Across the boundaries Γ_1 and Γ_2 the components of velocity normal to the surfaces (Γ_1 and Γ_2) are continuous. There exist velocity discontinuities parallel to these surfaces and of the following magnitudes:

Along Γ_1

$$\Delta v = v_f \sin \theta \tag{8a}$$

Along Γ_2

$$\Delta v = v_o \sin \theta \tag{8b}$$

Since the die is at rest, the velocity discontinuities along the conical surface Γ_3 and the cylindrical surface Γ_4 are as follows:

Along Γ_3

$$\Delta v = v_f r_f^2 \frac{\cos \alpha}{r^2} \tag{8c}$$

Along Γ_4

$$\Delta v = v_f \tag{8d}$$

The above treatment of the spherical field is provided in Refs. 1 and 2 and in Chapter 8 of Ref. 3. The calculation of the internal power of deformation, shear and friction losses and power associated with front and back tensions led to the solution for the net front/back pull as follows:

$$\sigma = \frac{\sigma_{xf} - \sigma_{xb}}{\sigma_o} = f_1\left(\frac{R_o}{R_f}, \alpha, m, \frac{L}{R_f}\right) \tag{9a}$$

where for the spherical field the function f_1 is determined by Eq. 8.11 of Ref. 3 as follows:

$$\sigma = f_1\left(\frac{R_o}{R_f}, \alpha, m, \frac{L}{R_f}\right) = 2f(\alpha)\ln\frac{R_o}{R_f} + \tag{9b}$$

where $$\frac{2}{\sqrt{3}}\left[\frac{\alpha}{\sin^2\alpha} - \cot\alpha + m\cot\alpha\ln\left(\frac{R_o}{R_f}\right) + \frac{mL}{R_f}\right]$$

$$f(\alpha) = \frac{1}{\sin^2\alpha}\left[1 - \cos\alpha\sqrt{1 - \frac{11}{12}\sin^2\alpha} + \frac{1}{11\cdot 12}\ln\frac{1 + \sqrt{\frac{11}{12}}}{\sqrt{\frac{11}{12}}\cos\alpha + \sqrt{1 - \frac{11}{12}\sin^2\alpha}}\right]$$

The results from the spherical velocity field (Eq. (9b)) will be compared with other solutions.

1.2 The Trapezoidal Velocity Field

The trapezoidal velocity field also uses a spherical coordinate system (r, θ, ϕ) to calculate the power requirements.

A kinematically admissible velocity field is described in Fig. 4. As before, the wire is divided into three zones in which the velocity field is continuous. In zones I and III the velocities are v_0 and v_f respectively, and in either case have only axial components. As before, volume constancy dictates that

$$v_o R_o^2 = v_f R_f^2$$

Zone I, in which deformation has not begun, consists of the incoming rod and it is separated from zone II by the surface Γ_2. Surface Γ_2 is an inclined plane with cylindrical symmetry which makes an angle β with the axis of symmetry. Zone II, the deformation zone, is bounded by the surface of the die with a semicone angle α. Zone III, which consists of the outgoing product, is separated from zone II by an inclined surface Γ_1 which is parallel to Γ_2. In zone II, the velocity is, at all times, directed towards the apex O of the cone, with cylindrical symmetry. The angle β is a pseudoindependent

process parameter. In the spherical coordinate system, the velocity components (see Fig. 5) are;

$$\dot{U}_r = \frac{v_o \sin\beta}{\sin(\beta+\theta)} \cdot \frac{\ell_2^2}{x^2} ; \qquad \dot{U}_\theta = \dot{U}_\phi = 0 \tag{10}$$

By substituting for ℓ_2 and x in terms of r_o, α and β

$$\dot{U}_r = v_o \left(\frac{r_o}{r}\right)^2 \sin\beta \; \frac{\sin^2(\alpha+\beta)}{\sin^3(\theta+\beta)}$$

Across the boundaries Γ_1 and Γ_2 the components of velocities normal to the surfaces are continuous. There exist velocity discontinuities parallel to these surfaces which can be expressed as:

Along Γ_2

$$\Delta v = v_o \sin\beta \{ \cot\beta - \cot(\beta+\theta)\} \tag{11a}$$

Along Γ_1

$$\Delta v = v_f \sin\beta \{ \cot\beta - \cot(\beta+\theta)\} \tag{11b}$$

Since the die is at rest, the velocity discontinuities along the conical surface Γ_3 and cylindrical surface Γ_4 are:

Along Γ_3

$$\Delta v = \frac{v_o \sin\beta}{\sin(\beta+\alpha)} \cdot \frac{\ell_2^2}{x^2} \tag{11c}$$

Along Γ_4

$$\Delta v = v_f \tag{11d}$$

The calculations of the internal power of deformation, the shear and friction losses, and power associated with front and back tensions yield

$$\sigma = \frac{\sigma_{xf} - \sigma_{xb}}{\sigma_o} = \frac{4}{\sqrt{3}} \sin^2(\alpha+\beta) \frac{\sin\beta}{\sin^2\alpha} * g(\alpha,\beta) + 2\ln\left(\frac{R_o}{R_f}\right) \frac{\sin\beta}{\sin^2\alpha} \sin^2(\alpha+\beta)[I_1 - I_2]$$

$$+ \frac{2m}{\sqrt{3}} \ln\left(\frac{R_o}{R_f}\right) \frac{\sin\beta}{\sin\alpha \sin(\alpha+\beta)} + \frac{2m}{\sqrt{3}} \frac{L}{R_f} \qquad (12)$$

where

$$g(\alpha,\beta) = \cos\beta \{\csc^2(\alpha+\beta) - \csc^2\beta\}$$
$$+ \cos\beta \cot\beta \{\cot\beta - \cot(\alpha+\beta)\}$$
$$+ \frac{\sin\beta}{3} \{\cot^3\beta - \cot^3(\alpha+\beta)\} \qquad (13)$$

$$I_1 = \sqrt{3} \cos\beta \left[-\frac{\Delta \cos\phi}{2\sin^2\phi} + \frac{1}{3} \ln \left\{\frac{\Delta - \cos\phi}{\Delta + \cos\phi}\right\} \right]_{\phi=\beta}^{\phi=\alpha+\beta}$$

with $$\Delta = \sqrt{1 + \frac{1}{3}\sin^2\phi} \qquad (14a)$$

and

$$I_2 = \frac{\sin\beta}{9} \left[\frac{(3 + \sin^2\beta)^{3/2}}{\sin^3\beta} - \frac{(3 + \sin^2(\alpha+\beta)^{3/2}}{\sin^3(\alpha+\beta)} \right] \qquad (14b)$$

The derivation of this expression can be seen in the section entitled "The derivation of the solution for the trapezoidal velocity field."

Please note that any value of the pseudoindependent parameter β will lead to an upper bound solution for σ. Thus, β becomes a subject for optimization of Eq. (12).

2. Parallel Flow - the Triangular Velocity Field

The triangular velocity field for plane strain flow is described in Green's work.[8] A more general solution for plane strain is worked in Ref. 5. Kudo[10] suggested the same velocity field for axisymmetric flow and Kobayashi

executed this task in Ref. 9. The present description is from Ref. 7, where a more general solution is provided.

In the triangular velocity field, the surfaces of velocity discontinuity Γ_1 and Γ_2 are conical surfaces that meet at the axis of symmetry (see Fig. 6). The position of their intersection point along the axis of symmetry is temporarily assumed arbitrarily. Thus the distance ℓ_2 is called a pseudo-independent parameter. When the total power of deformation is computed, it will be minimized with respect to ℓ_2.

In zones I and III, the material moves as a rigid body with a constant velocity v_o or v_f, respectively, in the axial direction. In the zone of plastic deformation, zone II, the velocity is parallel to the surface of the die and has the following components (see Fig. 6)

$$\left.\begin{aligned} v_R &= - K \tan\alpha \left(1 + \frac{x}{R} \tan\alpha\right), \\ v_x &= K \left(1 + \frac{x}{R} \tan\alpha\right), \\ v_\theta &= 0. \end{aligned}\right\} \qquad (15)$$

The constant K is obtained by calculating the volumetric flow through the cross-section at $x = 0$, where $v_x = K$, and equating it with either $v_o R_o^2$ (the inflow) or $v_f R_f^2$ (the outflow).

$$K = v_f \left(\frac{R_f}{R_\gamma}\right)^2 = v_o \left(\frac{R_o}{R_\gamma}\right)^2, \qquad (16)$$

where R_γ is the radius of the die at $x = 0$.

The above pattern of deformation satisfies, by definition, the kinematical conditions along the surface of the die.

Volume constancy everywhere is easily verified from

$$\left.\begin{aligned} \dot{\varepsilon}_{RR} &= \frac{Kx\,\tan^2\alpha}{R^2}\ , \\ \dot{\varepsilon}_{\theta\theta} &= -\frac{K\,\tan\alpha}{R}\left(1+\frac{x}{R}\tan\alpha\right), \\ \dot{\varepsilon}_{xx} &= \frac{K\,\tan\alpha}{R}\ . \end{aligned}\right\} \qquad (17)$$

The treatment of the triangular velocity field that is described above and in Fig. 6 (see Ref. 7) led to the following solution for the front and back pull:

$$\sigma = \left[\left(\frac{\sigma_{xf}}{\sigma_o}\right) - \left(\frac{\sigma_{xb}}{\sigma_o}\right)\right]_T = \frac{\cot\alpha}{\sqrt{3}}\left[F_\alpha\left(\frac{R_o}{R_d}\right) - F_\alpha\left(\frac{R_f}{R_d}\right)\right]$$

$$+ \frac{\sin\alpha}{\sqrt{3}}\left[\frac{1}{\sin\beta_1\,\sin(\beta_1+\alpha)} + \frac{1}{\sin\beta_2\,\sin(\beta_2-\alpha)}\right]$$

$$+ \frac{2m}{\sqrt{3}}\left[\left(\frac{R_o}{R_d} - \frac{R_f}{R_d}\right)\cot\alpha + \frac{L}{R_f}\right], \qquad (18)$$

where

$$F_\alpha(Z) = \sqrt{\left[4\,\tan^2\alpha + (1-Z)^2\right]} - 2\,\tan\alpha + \operatorname{arcsh}\left(\frac{1-Z}{2\tan\alpha}\right)$$

$$+ \sqrt{(4\,\tan^2\alpha + 1)}\left[\operatorname{arcsh}(2\,\tan\alpha) - \operatorname{arcsh}\left(\frac{4\,\tan^2\alpha + 1 - Z}{2Z\tan\alpha}\right)\right], \qquad (19)$$

and the value of R_d is found by successive approximation as follows:

(a) $$\left(\frac{R_d}{R_o}\right)^{(o)} = \sqrt{\frac{R_f}{R_o}}\,\cos\alpha\,\sqrt{1 + 2m\,\frac{1-(R_f/R_o)}{1+(R_f/R_o)}} \qquad (20)$$

as the zero order of precision for R_d.

(b) Successive orders of approximations $R_d^{(k)}$, k = 1,2,..., are calculated from $R_d^{(k-1)}$:

$$\left(\frac{R_d}{R_o}\right)^{(k)} = \left(\frac{R_d}{R_o}\right)^{(k-1)} - \left(\frac{\psi}{\psi'}\right)^{(k-1)} , \tag{21}$$

where ψ is a function of R_d/R_o:

$$\psi\left(\frac{R_d}{R_o}\right) = \left(\frac{R_o}{R_d}\right)\left[1 + \frac{R_f}{R_o} + 2m\left(1 - \frac{R_f}{R_o}\right)\right] - \left(\frac{R_d}{R_o}\right)\left(1 + \frac{R_o}{R_f}\right)\sec^2\alpha$$

$$+ \sqrt{4\tan^2\alpha + \left(1 - \frac{R_o}{R_d}\right)^2} - \sqrt{4\tan^2\alpha + \left(1 - \frac{R_f}{R_d}\right)^2} \tag{22}$$

and

$$\psi' = \frac{d\psi}{d(R_d/R_o)} \tag{23}$$

by differentiation

$$\psi'\left(\frac{R_d}{R_o}\right) = -\left(\frac{R_o}{R_d}\right)^2\left[1 + \frac{R_f}{R_o} + 2m\left(1 - \frac{R_f}{R_o}\right)\right] - \left(1 + \frac{R_o}{R_f}\right)\sec^2\alpha$$

$$+ \frac{(R_o/R_d)^2[1 - (R_o/R_d)]}{\sqrt{4\tan^2\alpha + [1 - (R_o/R_d)]^2}} - \frac{[1 - (R_f/R_d)](R_f/R_d)^2(R_f/R_o)}{\sqrt{4\tan^2\alpha + [1 - (R_f/R_d)]^2}} \tag{24}$$

The ratio (ψ/ψ') is calculated for $(R_d/R_o)^{(k-1)}$. Also, from the geometry

$$\sin\beta_1 = \frac{1}{\sqrt{1 + (\ell_1/R_f)^2}} \tag{25}$$

where

$$\frac{\ell_1}{R_f} = -\cot\alpha + 2\frac{R_d}{R_f}\operatorname{cosec}(2\alpha) \tag{26}$$

and

$$\sin\beta_2 = \frac{1}{\sqrt{1 + (\ell_2/R_o)^2}} \tag{27}$$

where

$$\frac{\ell_2}{R_o} = \cot\alpha - 2\,\frac{R_d}{R_o}\,\mathrm{cosec}(2\alpha) \tag{28}$$

The upper-bound solution by the triangular field is a little bulkier than that by the spherical field, and iteration procedure for the determination of the parameter R_d is involved. The derivation is performed in Ref. 7.

The Derivation of the Solution for the Trapezoidal Velocity Field

The total power required for the process can be split up into parts:

a) The power loss due to shear at surfaces of velocity discontinuities Γ_1 and Γ_2 denoted by $\dot{W}_s$

b) The power loss due to friction along die surfaces Γ_3 and Γ_4 denoted by $\dot{W}_f$

c) The internal work of deformation denoted by $\dot{W}_i$.

a) Calculation of $\dot{W}_s$:

Along surface Γ_2 (Fig. 4) the velocity normal to the surface is continuous,

$$v_o \cos(90°-\beta) = \dot{U}_r \cos(90°-\beta-\theta) \tag{29}$$

Thus, $$\dot{U}_r = \frac{v_o \sin\beta}{\sin(\beta+\theta)} \tag{30}$$

and $$\Delta v|_{\Gamma_2} = v_o \sin(90°-\beta) - \dot{U}_r \sin(90°-\beta-\theta)$$

$$= v_o \sin\beta\,[\cot\beta - \cot(\beta+\theta)] \tag{31}$$

For any point on the surface Γ_2, using the law of sines

$$\frac{b}{\sin\theta} = \frac{\ell_2}{\sin(180°-\beta-\theta)}$$

or $$\frac{b}{\ell_2} = \frac{\sin\theta}{\sin(\beta+\theta)} \tag{32a}$$

we have

$$\frac{db}{\ell_2} = \frac{\sin(\beta+\theta)\cos\theta - \sin\theta\cos(\beta+\theta)}{\sin^2(\beta+\theta)}\, d\theta$$

$$= \frac{\sin\beta}{\sin^2(\beta+\theta)}\, d\theta \qquad (32b)$$

$$ds\big|_{\Gamma_2} = 2\pi\, b\sin\beta\, db$$

$$= (2\pi\, \ell_2^2 \sin^2\beta \sin\theta/\sin^3(\beta+\theta))\, d\theta \qquad (33)$$

and

$$\dot{W}_s\big|_{\Gamma_2} = \int_{\Gamma_2} \tau|\Delta v|\, ds \qquad (34)$$

$$= \frac{\sigma_o}{\sqrt{3}}\, v_o \sin\beta\, 2\pi\, \ell_2^2 \sin^2\beta \int_{\theta=0}^{\alpha} [\cot\beta - \cot(\beta+\theta)] \frac{\sin\theta}{\sin^3(\beta+\theta)}\, d\theta$$

$$= M \int_{\theta=0}^{\alpha} \frac{\sin\theta}{\sin^3(\beta+\theta)} [\cot\beta - \cot(\beta+\theta)]\, d\theta \qquad (35)$$

where $M = \frac{2\sigma_o}{\sqrt{3}}\, \pi\, v_o\, \ell_2^2 \sin^3\beta$ (36)

Put $(\theta+\beta) = \phi$ and $d\theta = d\phi$. Eq. (35) becomes

$$\dot{W}_s\big|_{\Gamma_2} = M \int_{\beta}^{\beta+\alpha} \frac{\sin(\phi-\beta)}{\sin^3\phi} [\cot\beta - \cot\phi]\, d\phi \qquad (37)$$

This expression results in four separate integrals each of which is integrable and leads to the final expression :

$$\dot{W}_s\big|_{\Gamma_2} = \frac{2\pi\sigma_o}{\sqrt{3}} v_o \ell_2^2 \sin^3\beta \Big[\cos\beta \{\csc^2(\alpha+\beta) - \csc^2\beta\}$$

$$+\cos\beta\cot\beta \{\cot\beta - \cot(\alpha+\beta)\} + \frac{\sin\beta}{3} \{\cot^3\beta - \cot^3(\alpha+\beta)\}\Big] \quad (38)$$

Since, $\ell_2^2 = \dfrac{R_o^2 \sin^2(\alpha+\beta)}{\sin^2\alpha \sin^2\beta}$,

$$\dot{W}_s\big|_{\Gamma_2} = \frac{\sigma_o}{\sqrt{3}} v_o R_o^2 \, 2\pi \frac{\sin^2(\alpha+\beta)}{\sin^2\alpha} \sin\beta \, [g(\alpha,\beta)] \quad (39)$$

Similarly,

$$\dot{W}_s\big|_{\Gamma_1} = \frac{\sigma_o}{\sqrt{3}} v_f R_f^2 \, 2\pi \frac{\sin^2(\alpha+\beta)}{\sin^2\alpha} \sin\beta \, [g(\alpha,\beta)] \quad (40)$$

and,

$$\dot{W}_s = \dot{W}_s\big|_{\Gamma_1} + \dot{W}_s\big|_{\Gamma_2} = \frac{4\pi}{\sqrt{3}} \sigma_o v_f R_f^2 \frac{\sin^2(\alpha+\beta)}{\sin^2\alpha} \sin\beta \, [g(\alpha,\beta)] \quad (41)$$

Calculation of the velocity field in zone II.

This is done by equating volume rates in zone I and zone II which should be identical if we consider a tubular channel indicated by $d\theta$.

$$\dot{V}\big|_I = 2\pi \, b\sin\beta \, db \, v_o \sin\beta$$

$$= 2\pi \sin^2\beta \, v_o \ell_2 \frac{\sin\theta}{\sin(\beta+\theta)} \ell_2 \frac{\sin\theta}{\sin^2(\beta+\theta)} \, d\theta \quad (42)$$

$$\dot{V}\big|_{II} = 2\pi R \, r d\theta \, \dot{U}_r$$

$$= \frac{2\pi\sin^2\beta}{\sin\theta} \frac{x^2\sin^2\theta}{\sin^2(\beta+\theta)} \, d\theta \, \dot{U}_r \quad (43)$$

Since

$$\dot{V}\big|_I = \dot{V}\big|_{II} ,$$

$$\dot{U}_r = \frac{v_o \sin\beta}{\sin(\beta+\theta)} \frac{\ell_2^2}{x^2} \quad (44)$$

b) Calculation of $\dot{W}_f$:

Along Γ_3 (the conical die surface)

$$\dot{U}_r\Big|_{\theta=\alpha} = \frac{v_o \sin\beta}{\sin(\beta+\alpha)} \frac{\ell_2^2}{x^2} \tag{45}$$

and

$$\dot{W}_f\Big|_{\Gamma_3} = \int_{\Gamma_3} \mathcal{T}|\Delta v| \, dA$$

From the law of sines (see Fig. 5),

$$\frac{ds}{\sin\beta} = \frac{dx}{\sin(180° - \beta - \theta)} = \frac{dx}{\sin(\beta + \alpha)}$$

Also

$$\frac{b}{\sin\alpha} = \frac{x}{\sin(\beta+\alpha)}$$

and the elemental area around the die wall (dA)

$$dA = 2\pi R ds = 2\pi \, b \sin\beta \, ds$$

$$= 2\pi \frac{x \sin\alpha}{\sin(\beta+\alpha)} \sin\beta \frac{\sin\beta}{\sin(\beta+\alpha)} \, dx$$

Thus,

$$\dot{W}_f\big|_{\Gamma_3} = \int_{x=\ell_1}^{\ell_2} \frac{m\sigma_o}{\sqrt{3}} \frac{v_o \sin\beta \ell_2^2}{\sin(\beta+\alpha)} \frac{2\pi \sin\alpha \sin^2\beta}{\sin^2(\beta+\alpha)} \frac{x}{x^2} dx$$

$$= \frac{m\sigma_o}{\sqrt{3}} \frac{v_o \sin^3\beta}{\sin^3(\alpha+\beta)} \sin\alpha \, 2\pi\ell_2^2 \ln\left(\frac{\ell_2}{\ell_1}\right) \tag{46}$$

From similar triangles $\frac{\ell_2}{\ell_1} = \frac{R_o}{R_f}$ (47)

and $\ell_2 = \frac{R_o \sin(\alpha+\beta)}{\sin\alpha \sin\beta}$

we have

$$\dot{W}_f\big|_{\Gamma_3} = \frac{m\sigma_o}{\sqrt{3}} v_f R_f^2 \, 2\pi \ln\left(\frac{R_o}{R_f}\right) \frac{\sin\beta}{\sin\alpha \sin(\alpha+\beta)} \tag{48}$$

$$\dot{W}_f\big|_{\Gamma_4} = \frac{m\sigma_o}{\sqrt{3}} v_f \, 2\pi \, R_f \, L \tag{49}$$

c) Calculation of $\dot{W}_i$:

In order to calculate the internal power of deformation, it is necessary to calculate the strain rate components, $\dot{\varepsilon}_{rr}$, $\dot{\varepsilon}_{\theta\theta}$, and $\dot{\varepsilon}_{\phi\phi}$. From Eq. (44)

$$\dot{U}_r = \frac{v_o \sin\beta}{\sin(\beta+\theta)} \frac{\ell_2^2}{x^2}$$

and from the law of sines $x = \frac{r \sin(\beta+\theta)}{\sin\beta}$

$$\dot{U}_r = \frac{v_o \ell_2^2 \sin^3\beta}{r^2 \sin^3(\beta+\theta)} \tag{50}$$

$$\dot{\varepsilon}_{rr} = \frac{\partial \dot{U}_r}{\partial r} = \frac{-2v_o \ell_2^2 \sin^3\beta}{r^3 \sin^3(\beta+\theta)} \tag{51a}$$

$$\dot{\varepsilon}_{\theta\theta} = \dot{\varepsilon}_{\phi\phi} = \frac{\dot{U}_r}{r} = \frac{v_o \ell_2^2 \sin^3\beta}{r^3 \sin^3(\beta+\theta)} \tag{51b}$$

$$\dot{\varepsilon}_{r\theta} = \frac{1}{2r} \frac{\partial \dot{U}_r}{\partial \theta} = \frac{-3}{2} \frac{v_o \ell_2^2 \sin^3\beta}{r^3} \frac{\cos(\beta+\theta)}{\sin^4(\beta+\theta)} \tag{51c}$$

All the other $\dot{\varepsilon}_{ij} = 0$ because of axial symmetry, and

$$\sqrt{\frac{1}{2}\dot{\varepsilon}_{ij}\dot{\varepsilon}_{ij}} = \sqrt{\frac{1}{2}\dot{\varepsilon}_{rr}^2 + \frac{1}{2}\dot{\varepsilon}_{\theta\theta}^2 + \frac{1}{2}\dot{\varepsilon}_{\phi\phi}^2 + \dot{\varepsilon}_{r\theta}^2}$$

$$= \frac{v_o \ell_2^2 \sin^3\beta}{2r^3 \sin^4(\beta+\theta)} \sqrt{9 + 3\sin^2(\beta+\theta)} \tag{52}$$

An elemental volume inside zone II can be written as

$$dv = 2\pi\, r\sin\theta\, r d\theta\, dr$$

For a given θ in zone II r goes from

$$\frac{\ell_1 \sin\beta}{\sin(\beta+\theta)} \text{ at } \Gamma_1 \quad \text{to} \quad \frac{\ell_2 \sin\beta}{\sin(\beta+\theta)} \text{ at } \Gamma_2$$

and

$$\dot{W}_i = \frac{2}{\sqrt{3}} \sigma_o \int_v \sqrt{\frac{1}{2}\dot{\varepsilon}_{ij}\dot{\varepsilon}_{ij}}\, dv$$

$$= 2\pi\, \sigma_o v_o \ell_2^2 \sin^3\beta \int_{\theta=0}^{\alpha} \int_{r=\frac{\ell_1 \sin\beta}{\sin(\beta+\theta)}}^{\frac{\ell_2 \sin\beta}{\sin(\beta+\theta)}} \frac{\sin\theta}{r \sin^4(\beta+\theta)} \sqrt{3 + \sin^2(\beta+\theta)}\, dr\, d\theta$$

$$= 2\pi\, \sigma_o v_o \ell_2^2 \sin^3\beta \ln\left(\frac{R_o}{R_f}\right) \int_{\theta=0}^{\alpha} \frac{\sin\theta}{\sin^4(\beta+\theta)} \sqrt{3 + \sin^2(\beta+\theta)}\, d\theta$$

$$= Q \int_{\theta=0}^{\alpha} \frac{\sin\theta}{\sin^4(\beta+\theta)} \sqrt{3 + \sin^2(\beta+\theta)}\, d\theta \tag{53}$$

where

$$Q = 2\pi\sigma_o v_o \ell_2^2 \sin^3\beta \ln\left(\frac{R_o}{R_f}\right) \tag{54}$$

Using the substitution $\beta + \theta = \phi$, and

$$\sin\theta = \sin(\phi-\beta) = \sin\phi\cos\beta - \cos\phi\sin\beta ,$$

$$\dot{W}_i = Q \left[\int_{\phi=\beta}^{\beta+\alpha} \frac{\cos\beta}{\sin^3\phi} \sqrt{3 + \sin^2\phi}\, d\phi - \int_{\phi=\beta}^{\alpha+\beta} \frac{\cos\phi\sin\beta}{\sin^4\phi} \sqrt{3 + \sin^2\phi}\, d\phi \right]$$

$$= Q\,[I_1 - I_2] \tag{55}$$

The solution of the integrals I_1 and II_2 yields

$$I_1 = \cos\beta * \sqrt{3} \int_{\phi=\beta}^{\beta+\alpha} \frac{\sqrt{1 + \frac{1}{3}\sin^2\phi}}{\sin^3\phi}\, d\phi$$

$$= \sqrt{3}\cos\beta \left[\frac{-\Delta\cos\phi}{2\sin^2\phi} + \frac{1}{3} \ln\left\{ \frac{\Delta - \cos\phi}{\Delta + \cos\phi} \right\} \right]_{\beta}^{\beta+\alpha} \tag{14a}$$

where

$$\Delta = \sqrt{1 + \frac{1}{3}\sin^2\phi}$$

and

$$I_2 = \sin\beta \int_{\phi=\beta}^{\beta+\alpha} \frac{\cos^4\phi}{\sin^4\phi} \sqrt{3 + \sin^2\phi}\, d\phi$$

$$= \frac{\sin\beta}{9} \left[\frac{(3 + \sin^2\beta)^{3/2}}{\sin^3\beta} - \frac{(3 + \sin^2(\alpha+\beta))^{3/2}}{\sin^3(\alpha+\beta)} \right] \tag{14b}$$

Substituting for α and ℓ_2, we have

$$\dot{W}_i = 2\pi\, \sigma_o v_f R_f^2 \sin\beta \frac{\sin^2(\alpha+\beta)}{\sin^2\alpha} \ln\left(\frac{R_o}{R_f}\right) \{I_1 - I_2\} \tag{56}$$

Applied powers:

for drawing

$$J^* = \pi v_f R_f^2 \sigma_{xf} \tag{57}$$

for extrusion

$$J^* = -\pi v_f R_f^2 \sigma_{xb} \tag{58}$$

Setting the applied powers equal to the upper bound on energies, it follows that

$$\sigma = \frac{\sigma_{xf} - \sigma_{xb}}{\sigma_o} = \frac{4}{\sqrt{3}} \sin^2(\alpha+\beta) \frac{\sin\beta}{\sin^2\alpha} * g(\alpha,\beta)$$

$$+ 2\ln\left(\frac{R_o}{R_f}\right) \frac{\sin\beta}{\sin^2\alpha} \sin^2(\alpha+\beta) \{I_1 - I_2\}$$

$$+ \frac{2m}{\sqrt{3}} \ln\left(\frac{R_o}{R_f}\right) \frac{\sin\beta}{\sin\alpha \sin(\alpha+\beta)} + \frac{2m}{\sqrt{3}} \frac{L}{R_f} \tag{12}$$

where the definition of $g(\alpha,\beta)$, I_1 and I_2 are given by Eqs. (13) and (14a,b) respectively.

When β is chosen to be $\pi/2$, Eq. (12) reduces to a simple expression for the upper bound on the net drawing stress,

$$\sigma = \frac{\sigma_{xf} - \sigma_{xb}}{\sigma_o} = 2F(\alpha)\, \ell n(R_o/R_f) + \frac{4}{3\sqrt{3}} \tan\alpha + \frac{2}{\sqrt{3}} m \left[\frac{\ell n(R_o/R_f)}{\sin\alpha \cos\alpha} + \frac{L}{R_f}\right], \tag{59}$$

where

$$F(\alpha) = \frac{1}{9\tan^2\alpha} \left[\left(1 + \frac{3}{\cos^2\alpha}\right)^{3/2} - 8\right] \tag{60}$$

and $F(\alpha=0) = 1$.

Note the similarity of Eq. (59) and Eq. (d) in Sec. 3.17.3 of Ref. 11, when the typographical error in the last term in Eq. (d) is corrected to read $4/(3\sqrt{3})\tan\alpha$.

DISCUSSION

The results presented above can be discussed effectively by comparison of solutions based on different velocity fields. The comparison between spherical and triangular fields has been given in Ref. 7. This discussion will be restricted to a comparison of spherical and trapezoidal fields made on the following bases:

(i) Lowest upper-bound solution (UBS)

For most values of the semicone angle α, the relative stresses predicted by the spherical and trapezoidal fields are almost identical. This is shown qualitatively in Fig. 7. The values are so close to each other that the two curves overlap and fail to bring out the differences that exist. In order to see the nature of the relative differences, a differential plot was used. The ordinate was $[J(0) - J(\triangle)]/J(0)$. Figure 8 shows such a plot for $r = 25\%$ for different values of friction factor. The plot indicates that for small values of α, the trapezoidal field predicts a lower upper-bound solution; but as α increases the spherical field takes over. This crossover point of α increases with increasing values of the friction factor.

(ii) Simplicity of the derived expression that provides the UBS.

Looking at the final expressions yielded by these two velocity fields, it is rather obvious that the spherical field yields a solution that is less complex. This arises partly from the geometry of the surfaces of velocity discontinuities and partly from the fact that it is necessary to introduce a pseudoindependent variable in the case of a trapezoidal field solution.

(iii) Ease of derivation.

Here again the spherical field takes an upper hand. Not only is there a pseudoindependent variable associated with the calculation of the trapezoidal field, but this further necessitates an optimization step with respect to the pseudoindependent variable β.

It may be noted that although the solution to the trapezoidal field is somewhat cumbersome, all the integrals involved can be evaluated analytically. The only source of error would be the optimization step, which is done numerically. The error can, however, be made insignificant by carrying the optimization through the computer till a desired level of accuracy is attained. Figure 9 shows how the optimized pseudoindependent variable β varies as a function of α the semicone angle of the die.

In conclusion, the trapezoidal field predicts the lowest upper-bound solution for small values of α. As alpha values increase (see Fig. 7), the spherical field, the triangular field, and again, the spherical field, in turn become dominant.

ACKNOWLEDGEMENT

This work was initiated as a term paper in a graduate course (Spring 1979) on metal forming in the Department of Metallurgy and Materials Engineering at Lehigh University, and was partially supported by DOE project number DE-AC02-79ER10367.

REFERENCES

1 Avitzur, B., "Analysis of Wire Drawing and Extrusion Through Dies of Small Cone Angle," J. of Eng. for Ind., Trans. ASME, Series B, Vol. 85, Feb. 1963, pp. 89-96.

2 Avitzur, B., "Analysis of Wire Drawing and Extrusion Through Dies of Large Cone Angle," J. of Eng. for Ind., Trans. ASME, Series B, Vol. 86, Nov. 1964, pp. 305-316.

3 Avitzur, B., Metal Forming: Processes and Analysis, Original Edition, McGraw-Hill Book Company, 1968, 500 pages. Reprint with revisions and corrections, Robert E. Krieger Publishing Co., Inc. (645 New York Ave., Huntington,N.Y.11743), 1979, 498 pages.

4 Kiuchi, M. and Avitzur, B., "Limit Analysis of Flow Through Inclined Converging Planes," Proceedings of the 1978 Japan Spring Conf. for Technology of Plasticity Sponsored by Japan Society for Technology of Plasticity (JSTP) and Japan Society, for Mech. Engrg. (JSME), May 17-19, 1978, Hiroshima, Japan, Paper No. 420, pp. 533-538.

5 Kiuchi, M. and Avitzur, B., "Limit Analysis of Flow Through Inclined Converging Planes," ASME Paper No. 79-WA/PROD-10, Presented at the ASME Winter Annual Meeting in N.Y. on Dec. 3, 1979. To be published in the Transactions.

6 Avitzur, B; Iobst, J.; and McDermott, R. P.; "Axisform--A Computer Simulation Program for Axisymmetric Forging and Extrusion," Proceedings of the VI NAMRC (North American Metalworking Conf.), Gainsville, Florida, April 1978, pp. 174-179.

7 Avitzur, B.; Hahn, W.C.,Jr.; and Iscovici, S.; "Limit Analysis of Flow Through Conical Converging Dies," Journal of the Franklin Institute, Vol. 299, No. 5, May 1975, pp. 339-358.

8 Green, A.P., "Calculation of the Theory of Sheet Drawing," British Iron and Steel Research Assoc. Rep. MW/B/7/52, April 1952.

9 Kobayashi, S., "Upper-Bound Solutions of Axisymmetric Forming Problems - I," J. of Eng. Ind., Trans. ASME, pp. 326-332, Nov. 1964.

10 Kudo, H., "Some Analytical and Experimental Studies of Axisymmetric Cold Forging and Extrusion, Parts I and II, International J. of Mech. Sc., Vol. 2, pp. 102-127, 1960, and Vol. 3, pp. 91-117, 1961.

11 Avitzur, B., Metal Forming: The Application of Limit Analysis, Marcel Dekker, Inc., New York, N.Y., Jan. 1980, 224 pp.

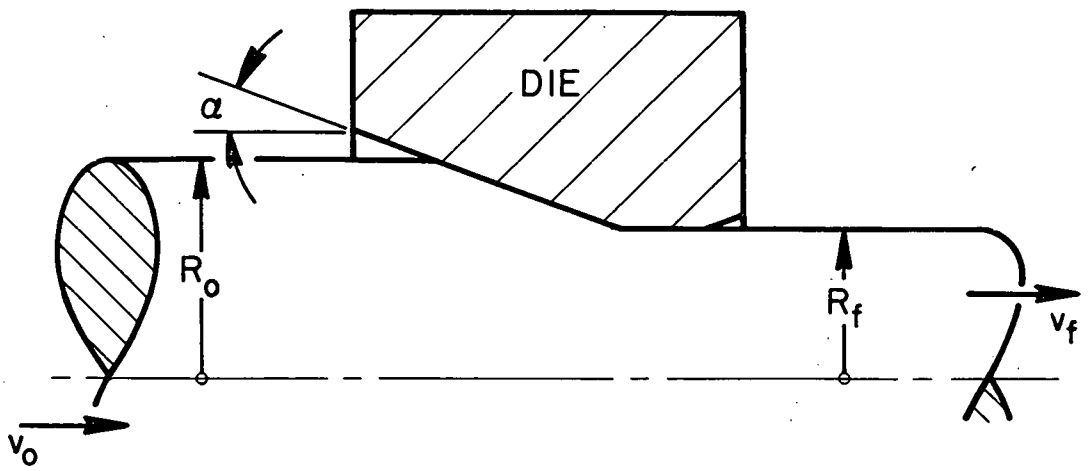

(a) THE DIE AND THE WORKPIECE .

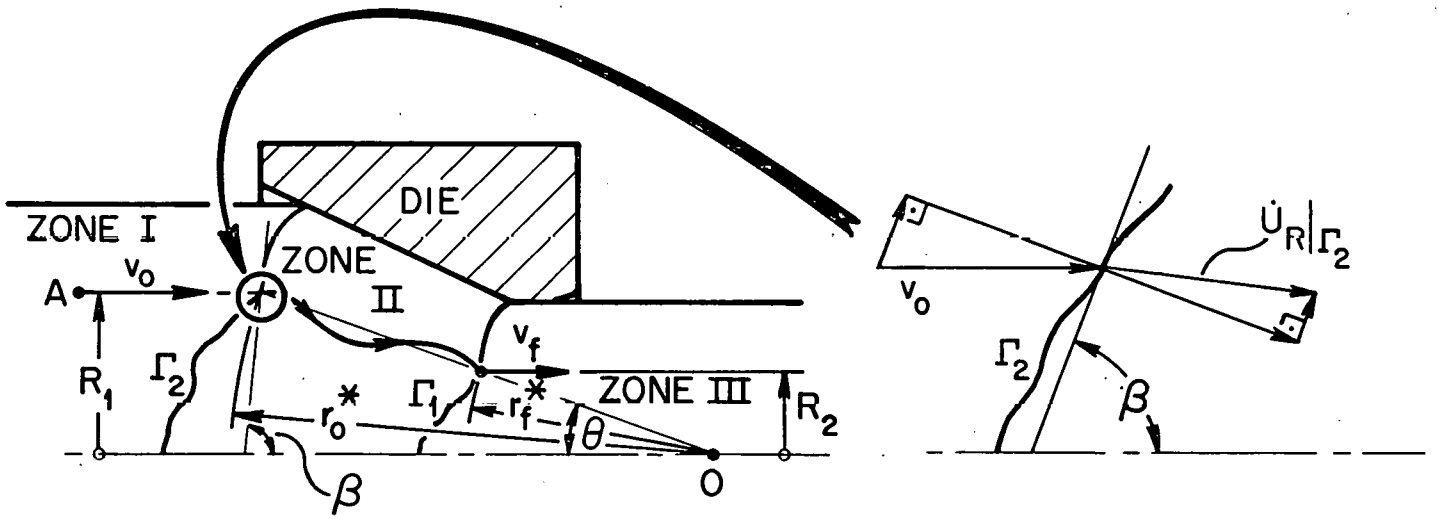

(b) FLOW AND SURFACES OF DISCONTINUITY.

FIG. 1 WIRE AND DIE .

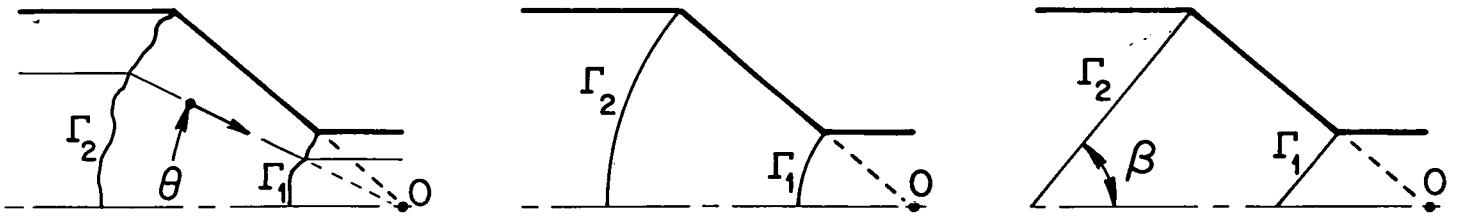

(a) CONICALLY CONVERGING RADIAL FLOW.

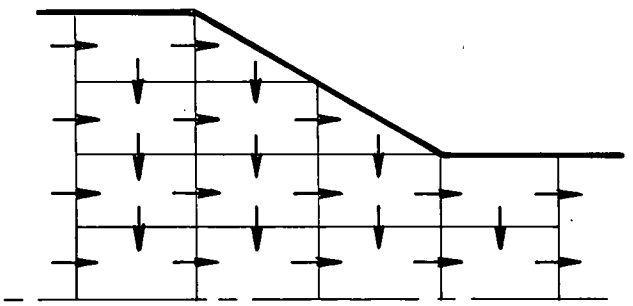

(b) CYLINDRICALLY CONVERGING RADIAL FLOW.

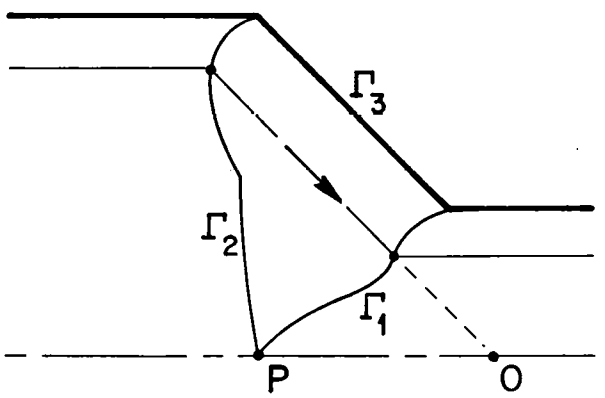

(c) PARALLEL FLOW

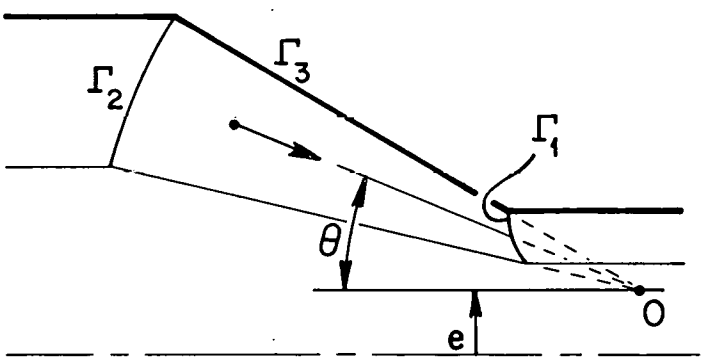

(d) TOROIDAL FLOW

FIG.2 BASIC VELOCITY FIELDS.

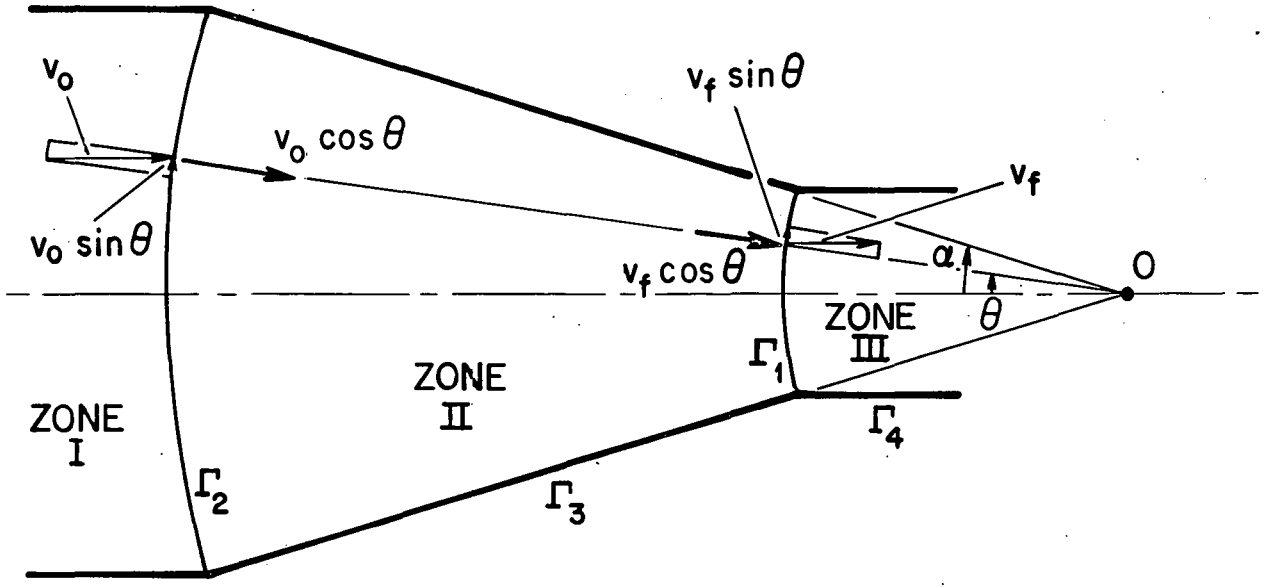

FIG.3 THE SPHERICAL VELOCITY FIELD.

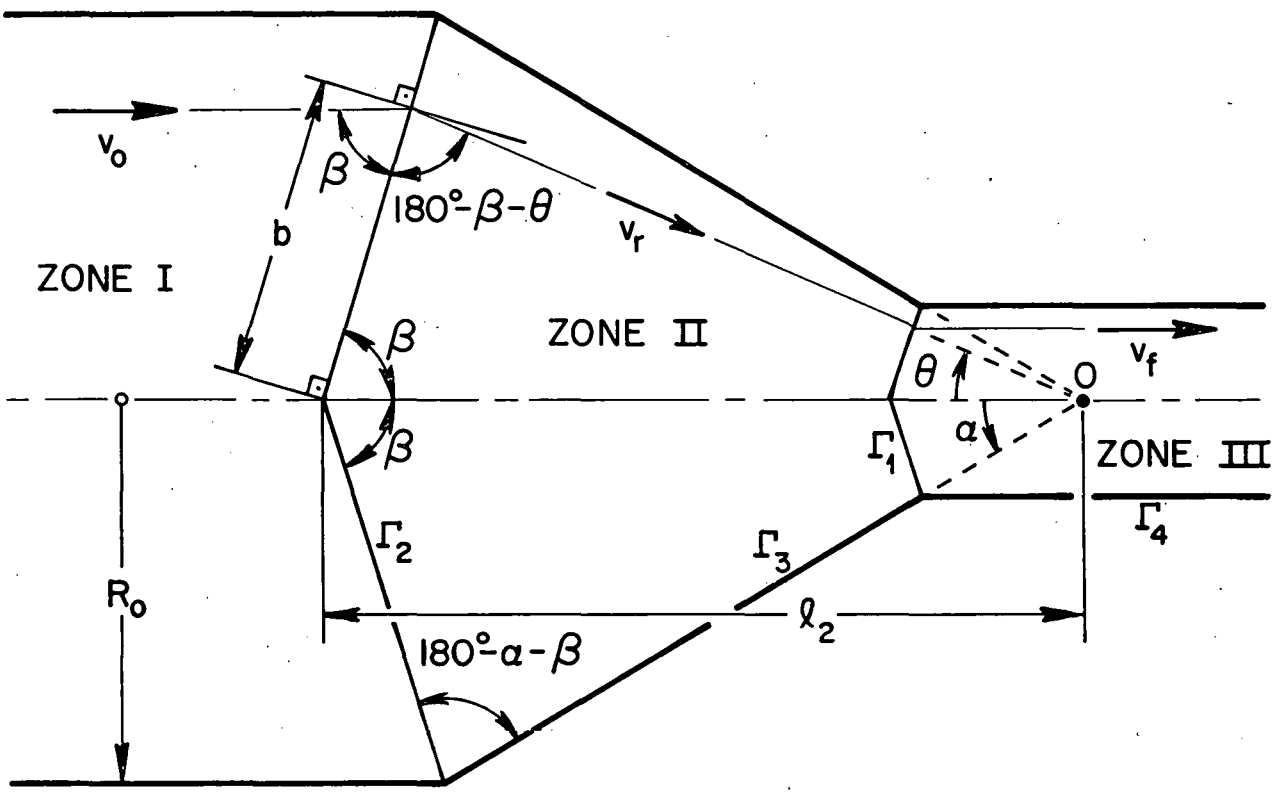

FIG.4 THE TRAPEZOIDAL VELOCITY FIELD.

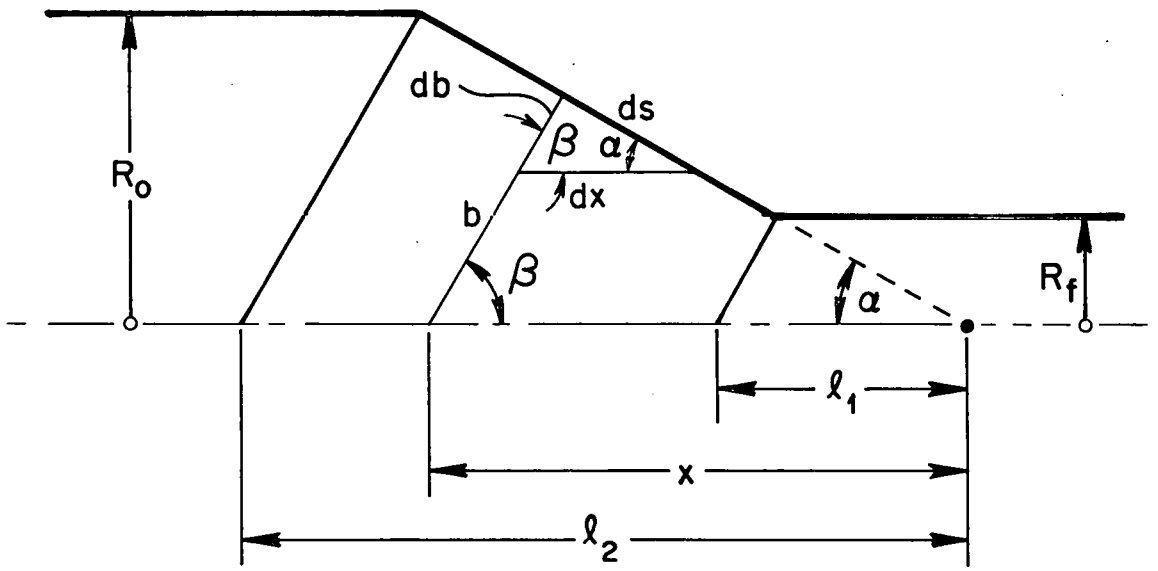

FIG.5 DERIVATION OF THE TRAPEZOIDAL VELOCITY FIELD.

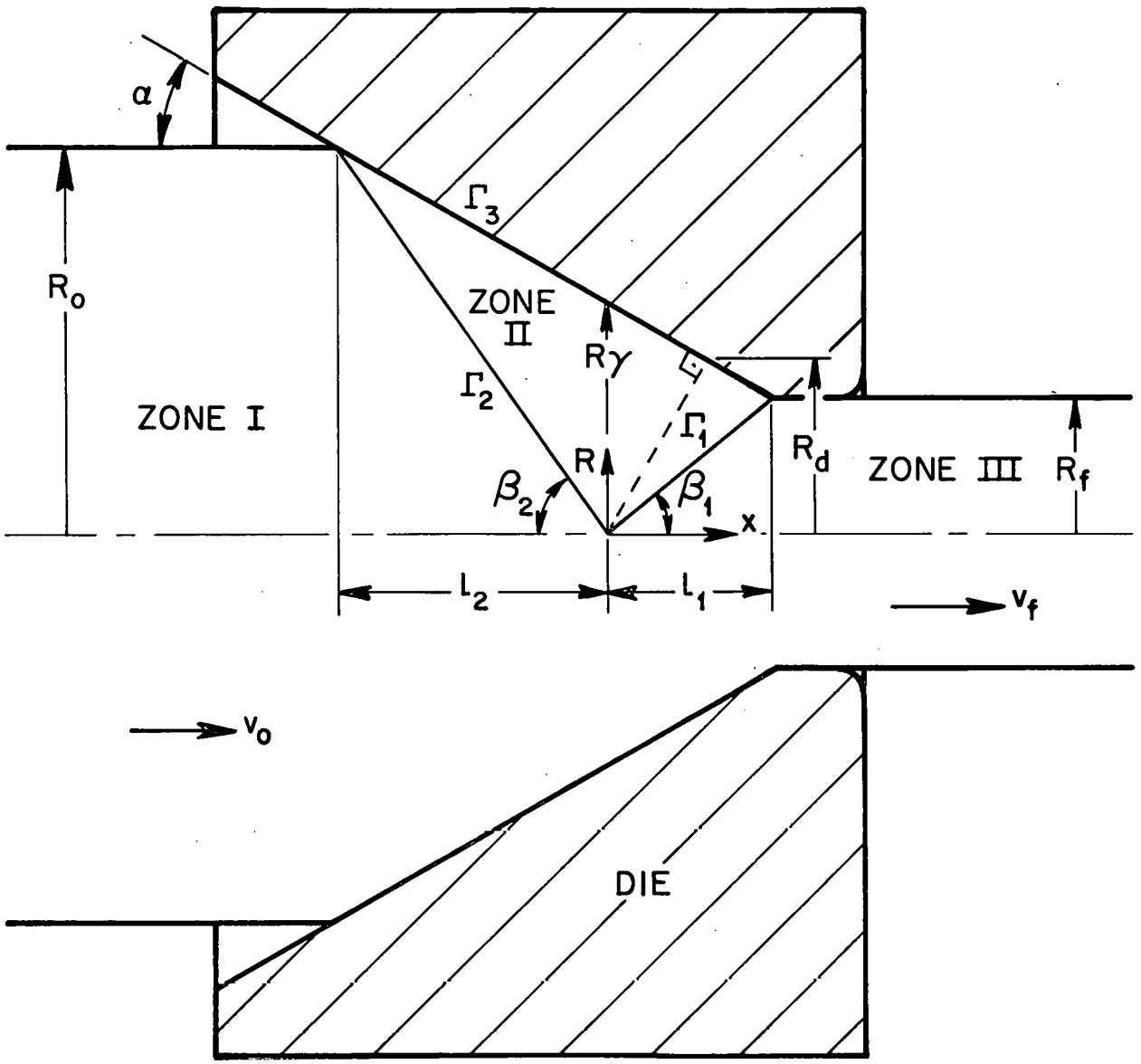

FIG.6 THE TRIANGULAR VELOCITY FIELD.

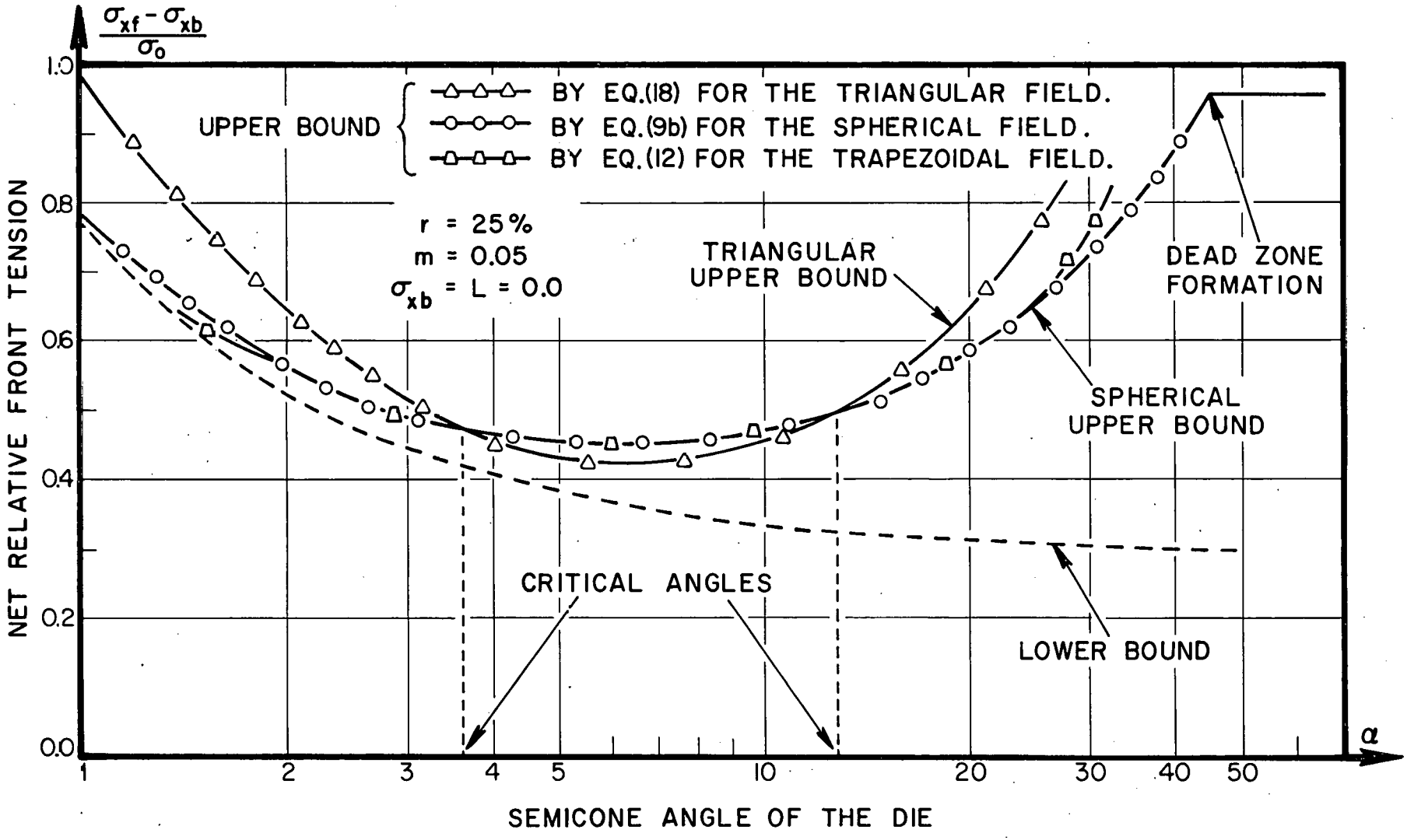

FIG.7 COMPARISON OF UPPER BOUND SOLUTIONS.

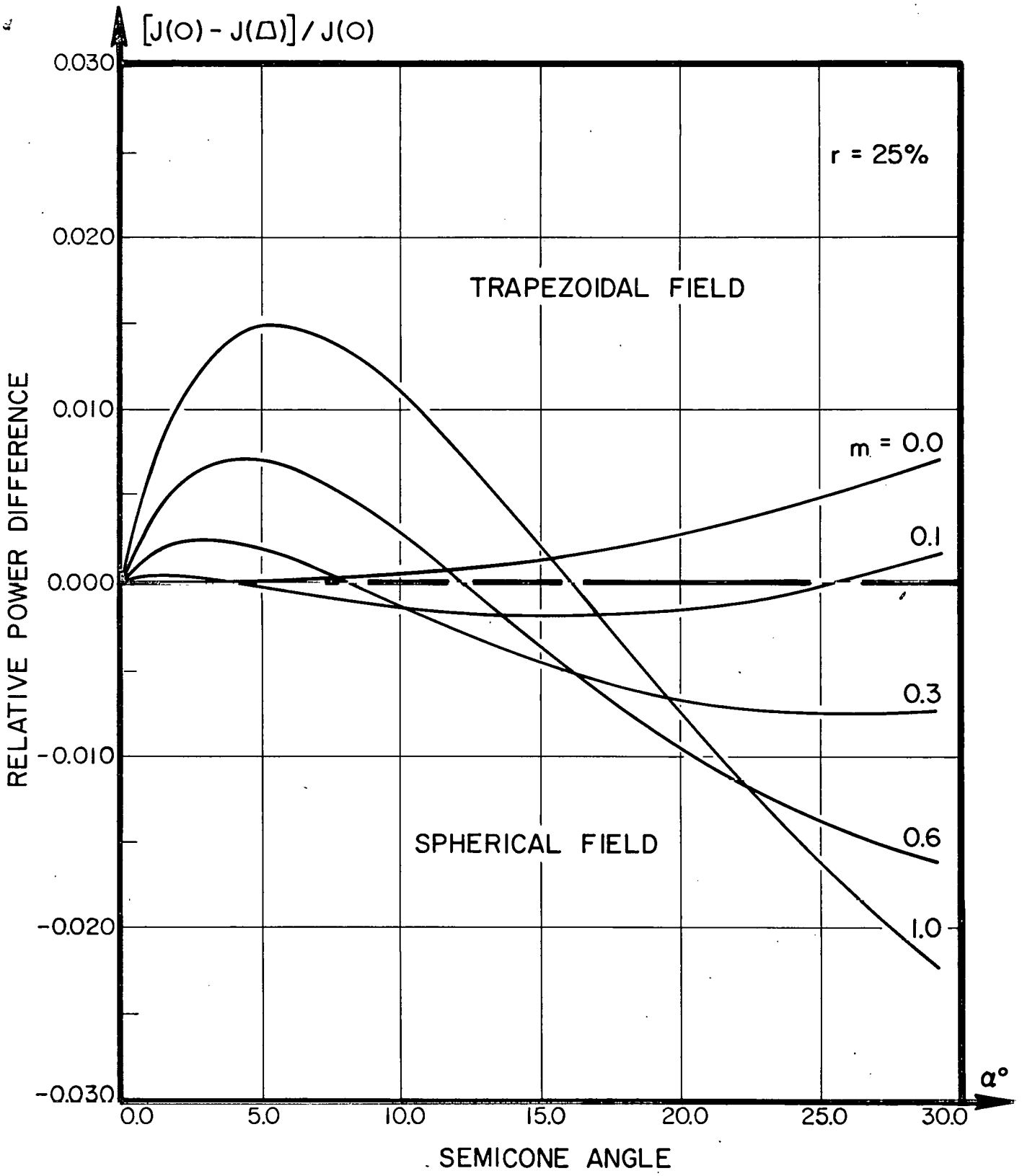

FIG.8 COMPARISON OF SPHERICAL AND TRAPEZOIDAL FIELDS.

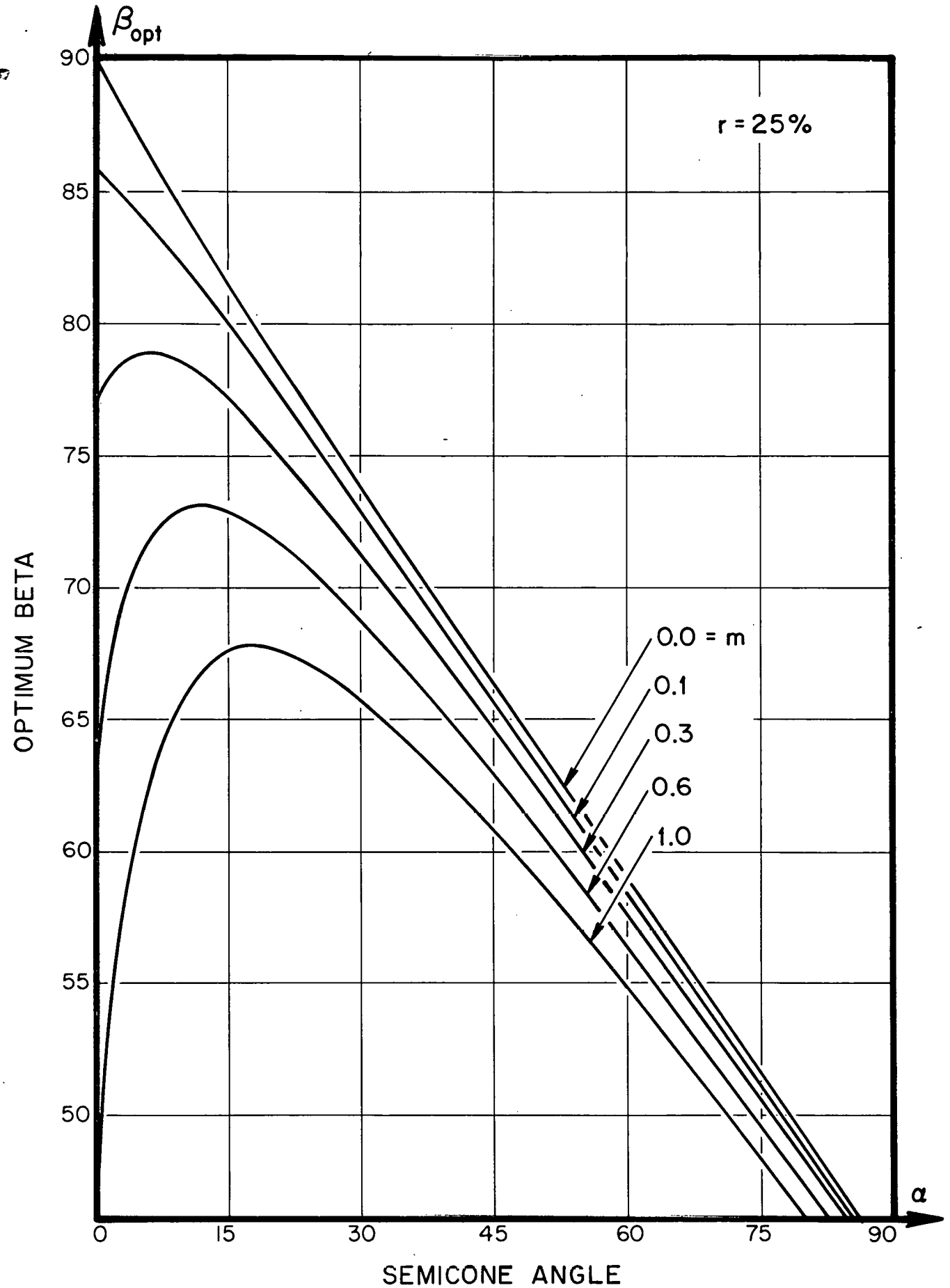

FIG.9 OPTIMUM β AS A FUNCTION OF SEMICONE ANGLE (α) AND FRICTION (m).